Supplementary Information

Visible Light-Triggered Fluorescence and pH Modulation using Metastable-state Photoacid and BODIPY

Parth K. Patel,[a] Juan E. Arias,[a] Renan S. Gongora,[a] Florencio E. Hernandez,[a,b], Aurélien Moncomble,[c] Stéphane Aloïse,[c] and Karin Y. Chumbimuni-Torres[a*]

a. Department of Chemistry, University of Central Florida, Orlando, FL 32816-2366, USA.
Email: Karin.ChumbimuniTorres@ucf.edu
b. The College of Optics and Photonics (CREOL), University of Central Florida, Orlando, FL 32816-2366, USA.
c. Univ. Lille, CNRS, UMR 8516 - LASIR - Laboratoire de Spectrochimie Infrarouge et Raman, F-59000 Lille, France.

Abstract: Small changes in the pH gradient play a critical role in numerous biological and chemical pathways. System capable of monitoring and regulating these changes with high sensitivity and minimum photo-fatigue are in demand. Herein, we propose a visible light-triggered molecular system that allows to reversibly regulate acidity and fluorescence. This robust bi-functional system opens new horizon towards novel studies that rely on small changes in acid mediated controlled processes with high sensitivity. The two photosensitive compounds employed, a metastable-state photoacid (*m*PAH) and a boron-dipyrromethene (BODIPY) derivatives, allow for consistent modulation of both fluorescence (based on the working principle of inner filter effect) and pH (around a magnitude) over multiple cycles.

Table of Contents

1. Experimental Section

Materials and Instrumentation

Acetone, dichloromethane (DCM), hexanes, ethyl acetate, methanol, ethanol, glacial acetic acid, hydrochloric acid (HCl), sodium hydroxide (NaOH) and sodium bicarbonate were purchased from Fisher, USA. Benzoyl chloride, 2,4-dimethylpyrrole, boron trifluoroetherate, glycine, acetonitrile, and 2-ethylhexyl bromide were purchased from Acros, USA. 2,4-dihydroxybenzaldehyde and cyclohexyl methyl ketone were purchased from Alfa Aesar, USA. Phenyl hydrazine hydrochloride was purchased from TCI, USA. Potassium carbonate (K_2CO_3), tris(hydroxymethyl)aminomethane (Tris) and sodium sulfate were purchased from Amresco, USA. Potassium iodide (KI), sodium chloride (NaCl), boric acid, phosphoric acid, 1,3-propanesultone and triethylamine were purchased from Sigma-Aldrich, USA. Deuterated NMR solvents were purchased from Cambridge Isotope Laboratories, Inc., USA. BODIPY was synthesized according to literature procedure.[1]

^{1}H and ^{13}C NMR spectroscopy were carried out with NMR spectrometer (Avance III 400) from Bruker, USA. Absorbance based experiments were performed using a UV-Vis spectrophotometer (Cary 50 Bio UV/Visible) from Varian, Australia. The source of visible light activation was a 470 nm 120 LED array (maximum average power of 1800 mW) from Elixa, USA. Deionized water used to prepare solutions for pH studies was purified by a water purification system with resistance of 18 MΩcm (Milli-Q Academic) from EMD Millipore Corporation, USA. The pH of the solutions was obtained with a pH meter (Orion Start A211) from Thermo Scientific, USA. Steady-state fluorescence experiments were performed using a spectrofluorometer (FluoroMax-4 Spectrofluorometer) from Horiba Scientific, USA. Time-resolved fluorescence (lifetime decay profiles) studies were performed using a spectrofluorometer (FLS980 Spectrometer) equipped with a 470 nm ± 10 nm picosecond pulsed diode laser as the excitation source (EPL – 470 with a maximum average power of 5 mW) from Edinburgh Instruments, UK. The excitation wavelength of diode laser (EPL – 470) was 470 nm (Δλ = 1 nm), pulse duration was 92 ps, pulse spacing was fixed at 200 ps, and pulse repetition rate was 5 MHz. The emission wavelength selected was 509 nm (Δλ = 1 nm) based on the steady-state fluorescence experiment. The fluorescence lifetime decay profiles were recorded until 2000 peak counts were reached for all ethanolic solutions (see Fig. S16 and Table S1 for concentrations used) at room temperature. The decay profiles were corrected with background (instrument response function) and processed to determine the lifetime values obtained by global analysis (reconvolution) fitting using FAST Version 3.4.2. Software (Edinburgh Instruments, UK). All experiments were carried out in the dark unless mentioned otherwise.

Synthesis

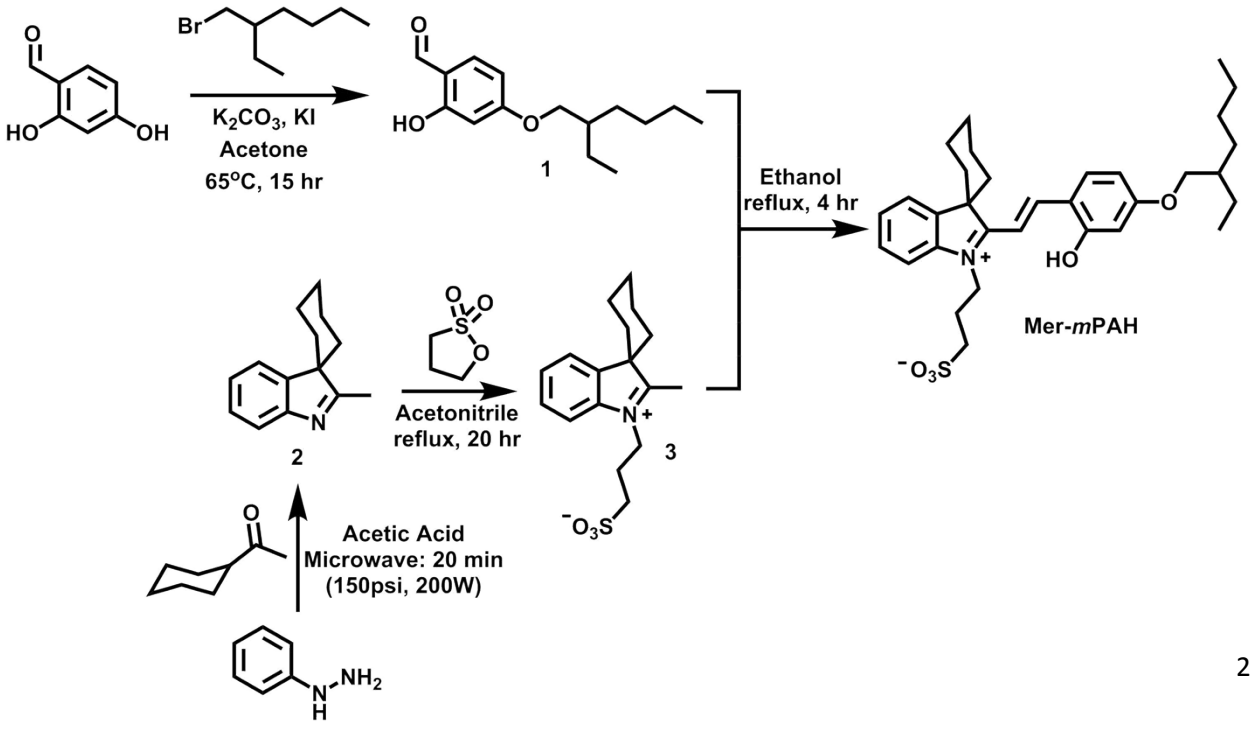

Scheme S1. Synthetic route used to prepare Mer-*m*PAH.

2-hydroxy-4-(2-ethylhexoxy)benzaldehyde (**1**): The synthesis of **1** was modified following literature procedure.[2] In a 50 mL two-neck flask, equipped with a stir bar and a reflux condenser, was charged with K_2CO_3 (0.506 g, 3.656 mmol) followed by flame drying and purging with nitrogen gas (three times) the equipment setup. Under nitrogen gas, 2,4-dihydroxybenzaldehyde (1.000 g, 7.240 mmol) and dry acetone (8 mL) were added to the reaction flask, followed by raising the temperature to 65ºC. After 20 minutes, a solution of KI (10%) and 2-ethylhexyl bromide (2.438 g, 7.312 mmol) in dry acetone (12 mL) was added dropwise to the reaction flask. After 15 hours, the reaction mixture was concentrated in vacuo, and excess 2-ethyl hexyl bromide was removed by distillation. The remaining organic residue was dissolved in minimal DCM and neutralized with 0.1 M HCl. The acid washes were extracted with DCM. Then, the organic phase was washed with brine (saturated NaCl), separated and passed through a drying column. After concentrating the organics in vacuo, the crude was purified by column chromatography (silica) in hexanes and eluted in 50% ethyl acetate in hexanes to afford a colorless oil. Yield (49%). ^{1}H NMR (400 MHz, $CDCl_3$): δ (ppm) = 11.48 (s, 1H), 9.70 (s, 1H), 7.42-7.40 (d, J = 8.67 Hz, 1H), 6.55-6.52 (dd, J = 2.32 Hz, J = 8.66 Hz, 1H), 6.42 (d, J = 2.29 Hz, 1H), 3.90-3.89 (d, J = 5.83 Hz, 2H), 1.77-1.71 (m, 1H), 1.53-1.30 (m, 10H), 0.95-0.91 (m, 6H). ^{13}C NMR (400 MHz, $CDCl_3$): δ (ppm) = 194.24, 166.69, 164.53, 135.14, 114.98, 108.80, 101.07, 71.05, 39.13, 30.40, 29.00, 23.77, 22.99, 11.04.

2'-methylspiro[cyclohexane-1,3'-[3H]indole] (**2**): The synthesis of **2** was modified following literature procedure.[3] In a 30 mL microwave reaction flask, equipped with a stir bar, was charged with cyclohexyl methyl ketone (1.003 g , 7.949 mmol) and glacial acetic acid (13.93 mL). This reaction mixture was sonicated for few minutes before adding phenyl hydrazine hydrochloride (1.138 g, 7.870 mmol). After 20 mins of microwave irradiation (150 psi, 200W), glacial acetic acid was removed in vacuo to result an orange residue. This residue was dissolved in DCM and neutralized with sodium bicarbonate. The organic phase was separated and washed three times with brine. Then, the organic phase was collected, dried with anhydrous sodium sulfate and the DCM was removed in vacuo to afford a red brown oil. Yield (77%). ^{1}H NMR (400 MHz, $CDCl_3$): δ (ppm) = 7.71-7.69 (d, J = 7.36 Hz, 1H), 7.56-7.54 (d, J = 7.54 Hz, 1H), 7.34-7.30 (td, J = 7.57 Hz, J = 15.21 Hz 1H), 7.17-7.13 (td, J = 7.48 Hz, J = 14.98Hz, 1H), 2.27 (s, 3H), 1.98-1.73 (m, 8H), 1.31-1.26 (m, 2H). ^{13}C NMR (400 MHz, $CDCl_3$): δ (ppm) = 187.65, 154.12, 144.48, 127.39, 124.14, 124.13, 120.00, 57.77, 31.06, 25.21, 21.51, 16.02.

2'-methyl-1'-(3-sulfopropyl)spiro[cyclohexane-1,3'-[3H]indolium] inner salt (**3**): The synthesis of **3** was modified following literature procedure.[4] In a 125 mL round bottom flask equipped with a stir bar, **2** (1.10 g, 5.517 mmol) dissolved in acetonitrile (55 mL) was added under nitrogen gas. Then, 1,3-propanesultone (0.741 g, 6.068 mmol) was added dropwise over a period of 30 minutes to the reaction mixture at room temperature under nitrogen gas. Afterwards, the reaction mixture was refluxed under nitrogen gas for 20 hours. Acetonitrile was then removed under vacuo and the crude was purified by column chromatography (silica) using 7% (v/v) methanol in DCM to remove unreacted 1,3-propanesultone. Both purple and brown fractions were combined and concentrated under vacuo, and used without further purification. NMR spectra could not be obtained. Crude yield (60 %).

Mer-*m*PAH: The synthesis of Mer-*m*PAH was modified following literature procedure.[5] In a 125 mL round bottom flask, crude **3** (0.200 g, 0.622 mmol) was dissolved in anhydrous ethanol (25 mL). Prior to immediate addition of **1** (0.267 g, 0.684 mmol) to the reaction mixture, it was first placed under high vacuum overnight. After addition, the reaction mixture was heated to reflux under nitrogen for 4 hours. Ethanol was removed in vacuo, and the residue was purified by column chromatography (silica, washed with 1% acetic acid in mobile phase) using 6% (v/v) methanol in DCM. All orange and pink fractions were collected and washed with aqueous 1.0 M HCl and extracted with DCM. The organic phase was separated and dried using anhydrous sodium sulfate. The clear reddish orange organic solution was concentrated in vacuo to afford a red solid. Yield (20%). ^{1}H NMR (400 MHz, DMSO-d_6): δ (ppm) = 11.34 (br. s, 1H), 8.76-8.72 (d, J = 16.16 Hz, 1H), 8.32-8.29 (d, J = 9.61 Hz, 1H), 8.13-8.11 (d, J = 7.43 Hz, 1H), 8.02-8.00 (d, J = 8.07 Hz, 1H), 7.66-7.60 (m, 2H), 7.53-7.49 (t, J = 7.48 Hz, J = 15.00 Hz, 1H), 6.59 (m, 2H), 4.78-4.74 (br. t, J = 7.36 Hz, J = 14.99 Hz, 2H), 3.95-3.93 (d, J = 5.46 Hz, 2H), 2.69-2.66 (br. t, J = 5.95 Hz, J = 12.15 Hz, 2H), 2.22-1.88 (m, 10H), 1.69-1.64 (m, 3H), 1.33-1.24 (m, 6H), 0.90-0.87 (m = 8H). ^{13}C NMR (400 MHz, DMSO-d_6): δ (ppm)

= 165.77, 161.66, 148.25, 141.74, 141.35, 128.89, 127.43, 125.46, 115.04, 114.80, 108.64, 106.97, 101.07, 70.56, 55.53, 47.31, 44.91, 38.37, 34.26, 29.72, 28.31, 24.27, 24.20, 23.12, 22.40, 20.60, 13.85, 10.79.

2. ^{1}H and ^{13}C NMR spectra for 1, 2 and Mer-*m*PAH

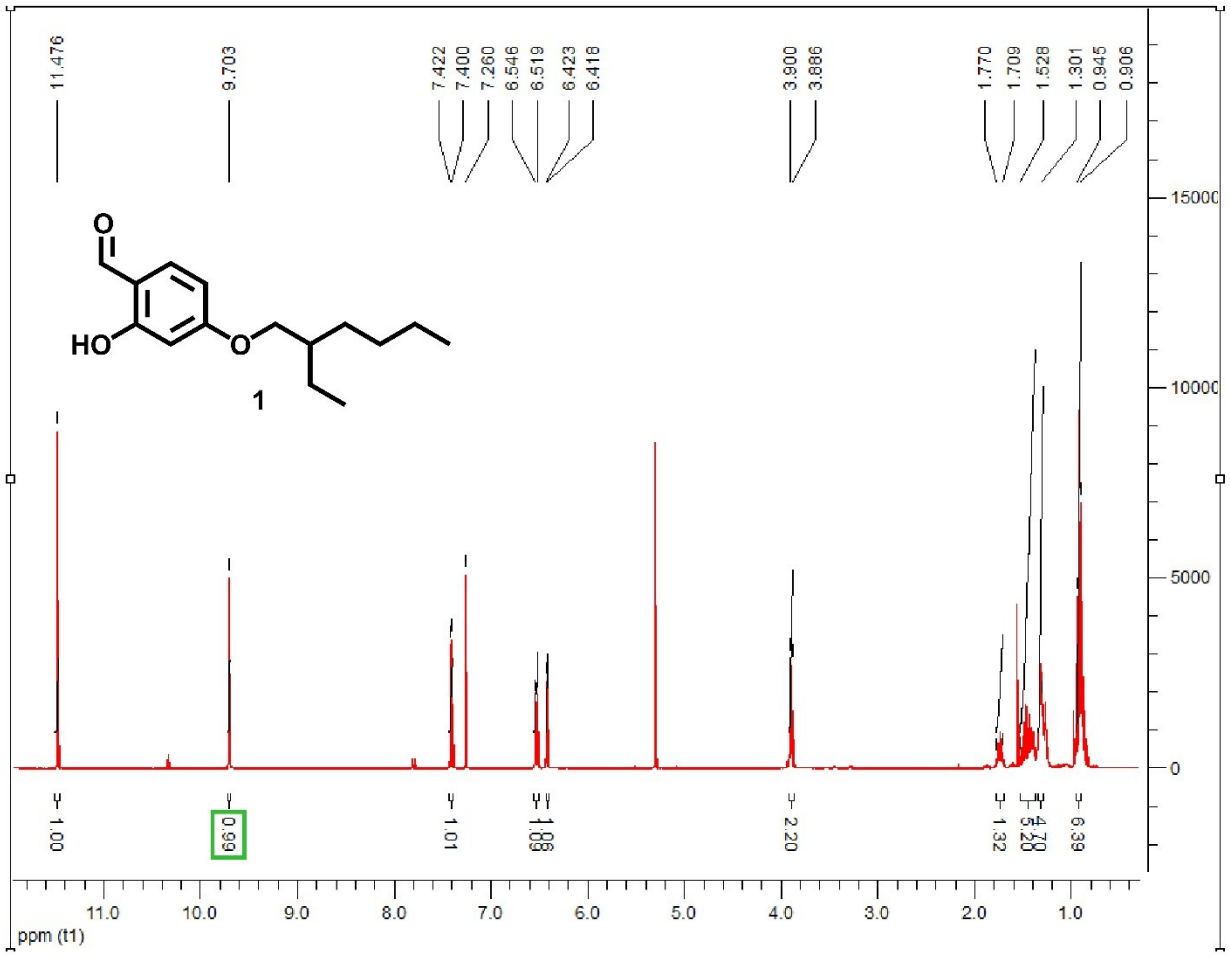

Fig. S1 ^{1}H NMR spectra of **1**.

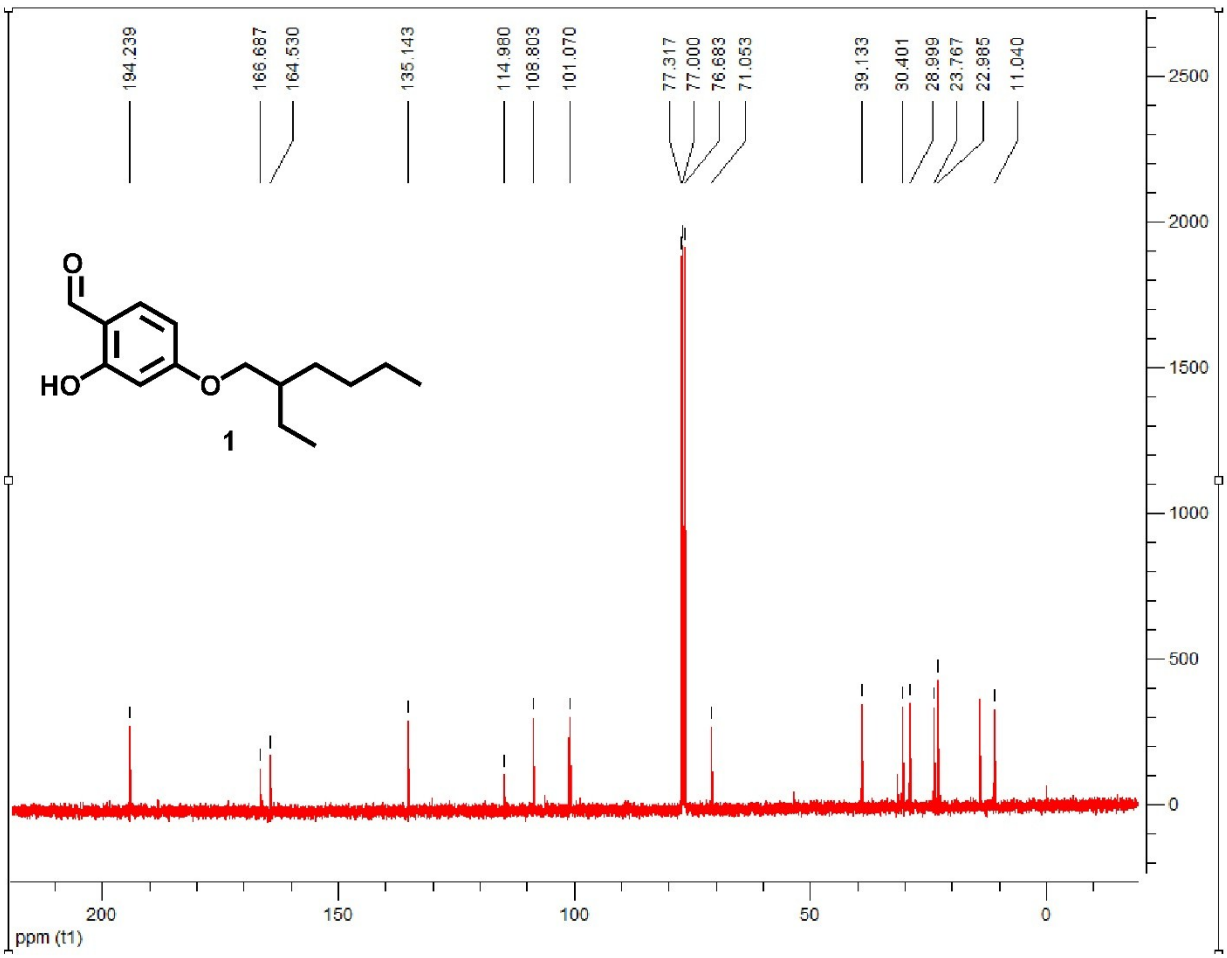

Fig. S2 ^{13}C NMR spectra of **1**.

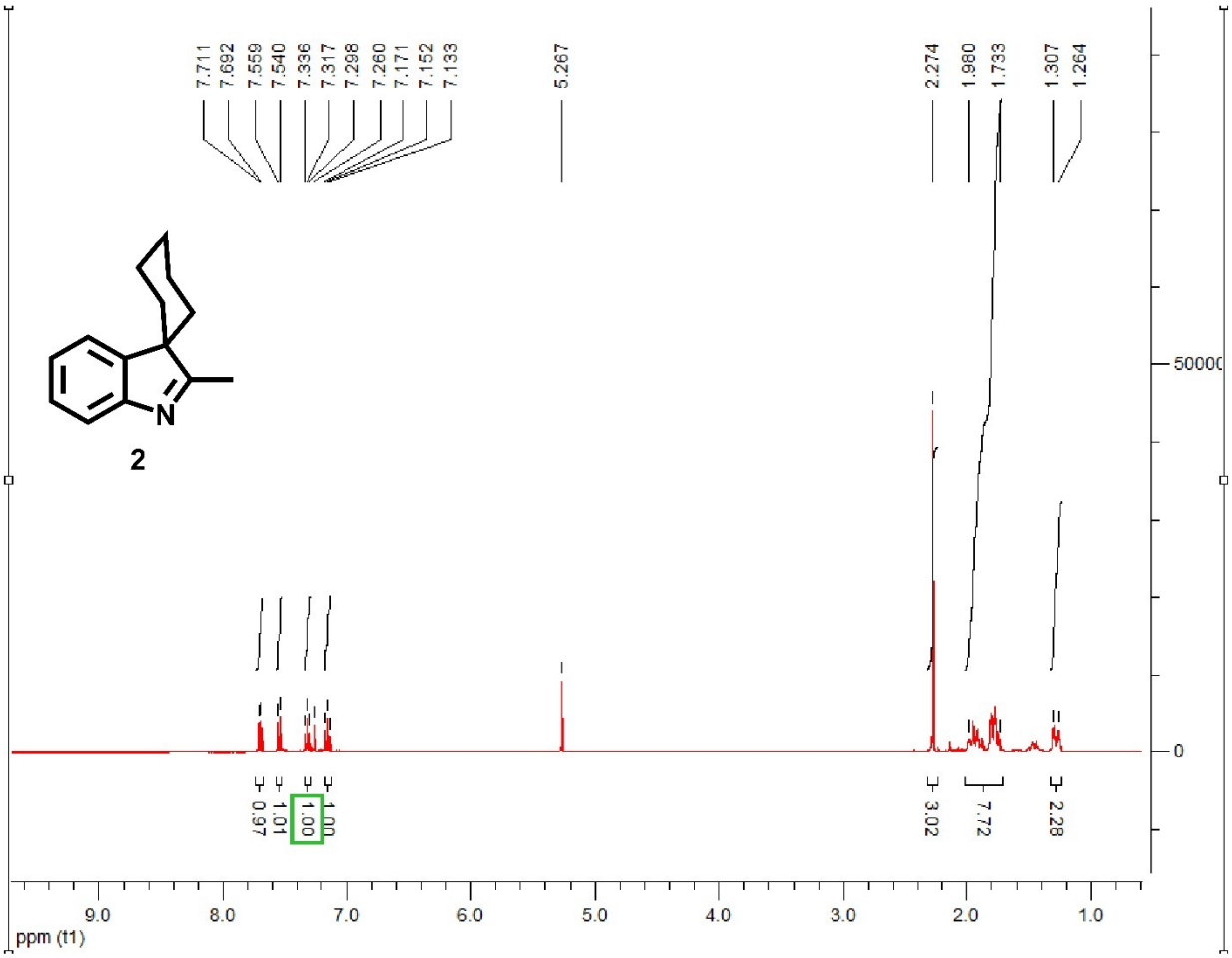

Fig. S3 ^{1}H NMR spectra of **2**.

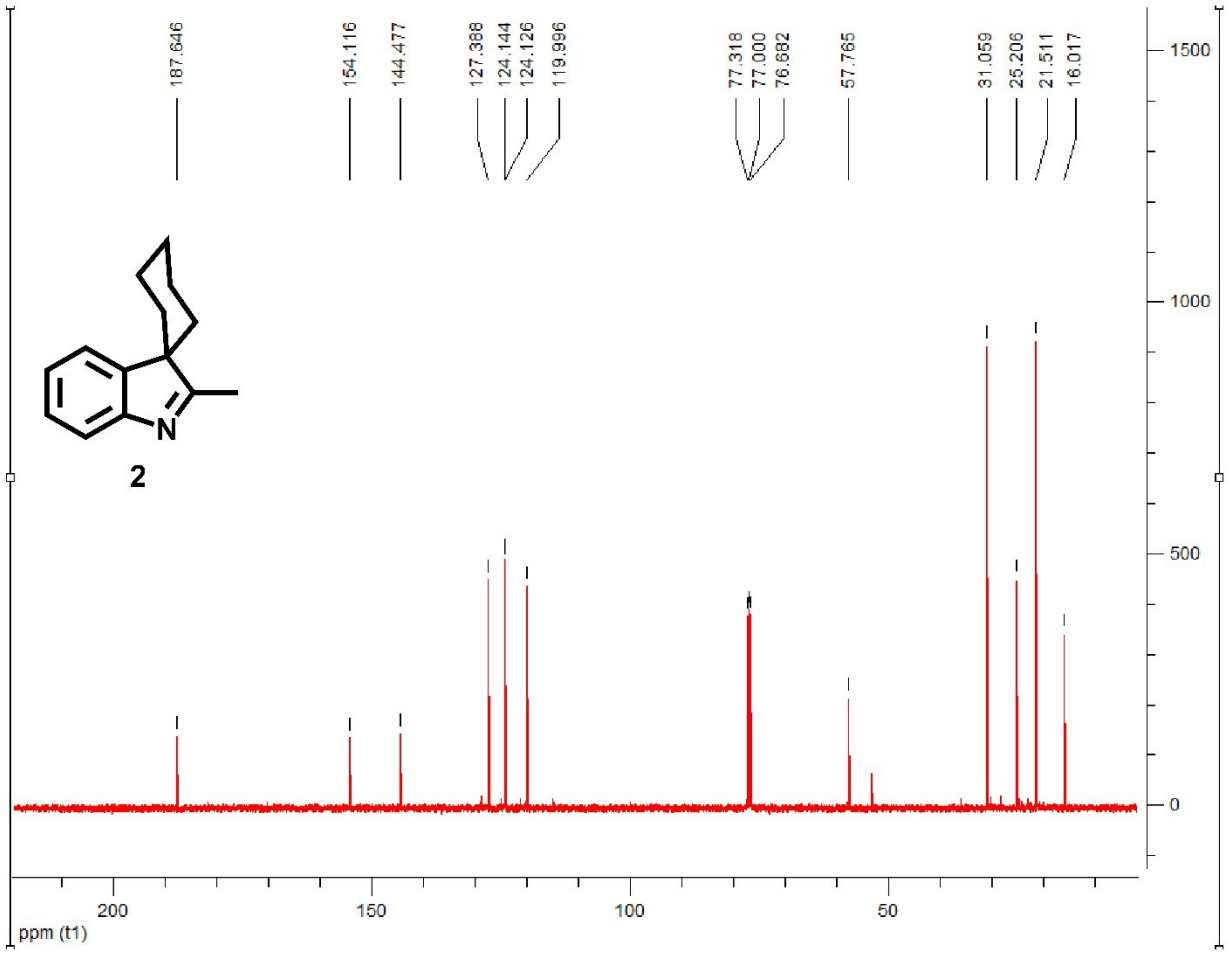

Fig. S4 ^{13}C NMR spectra of **2**.

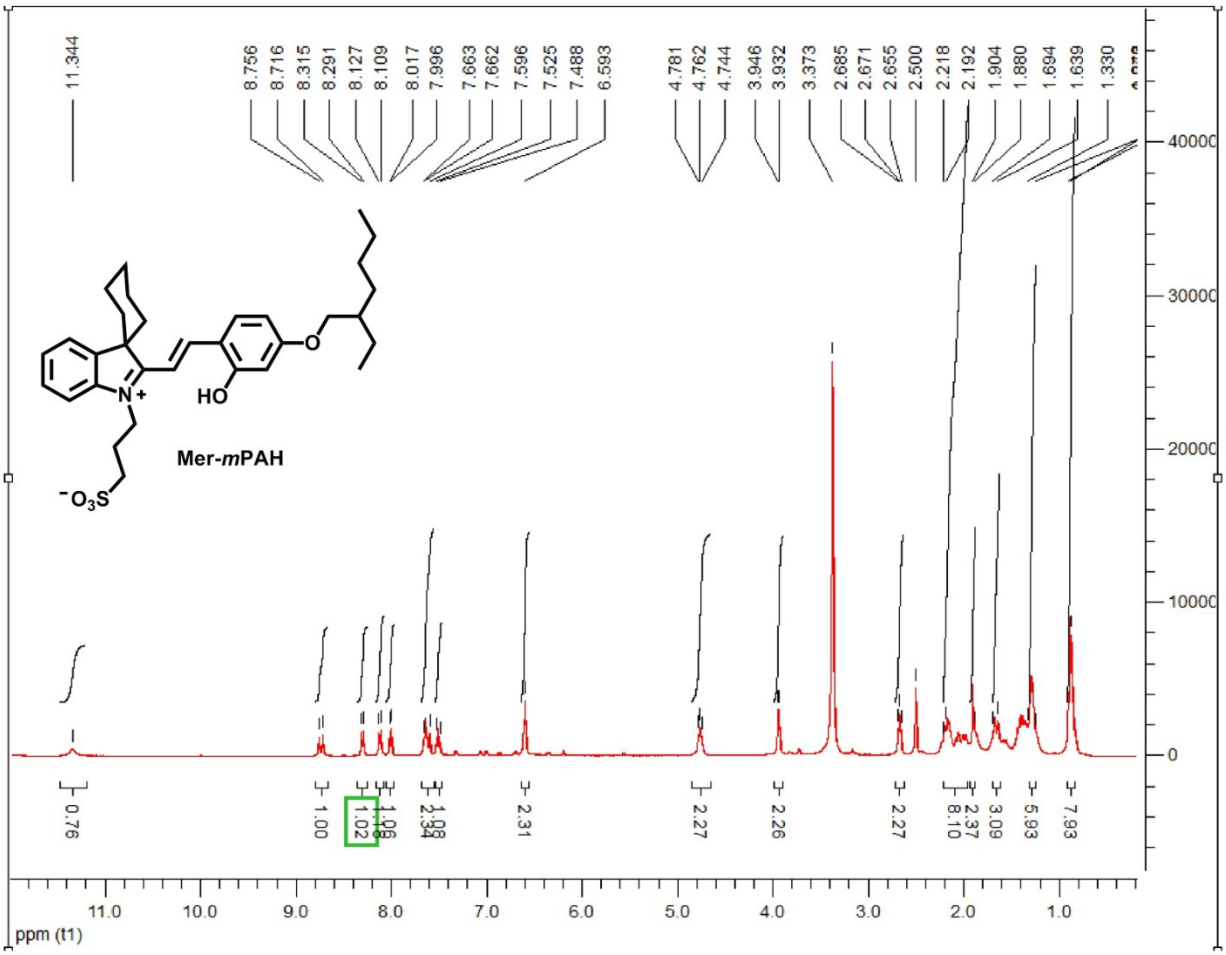

Fig. S5 ^{1}H NMR spectra of **Mer-*m*PAH**.

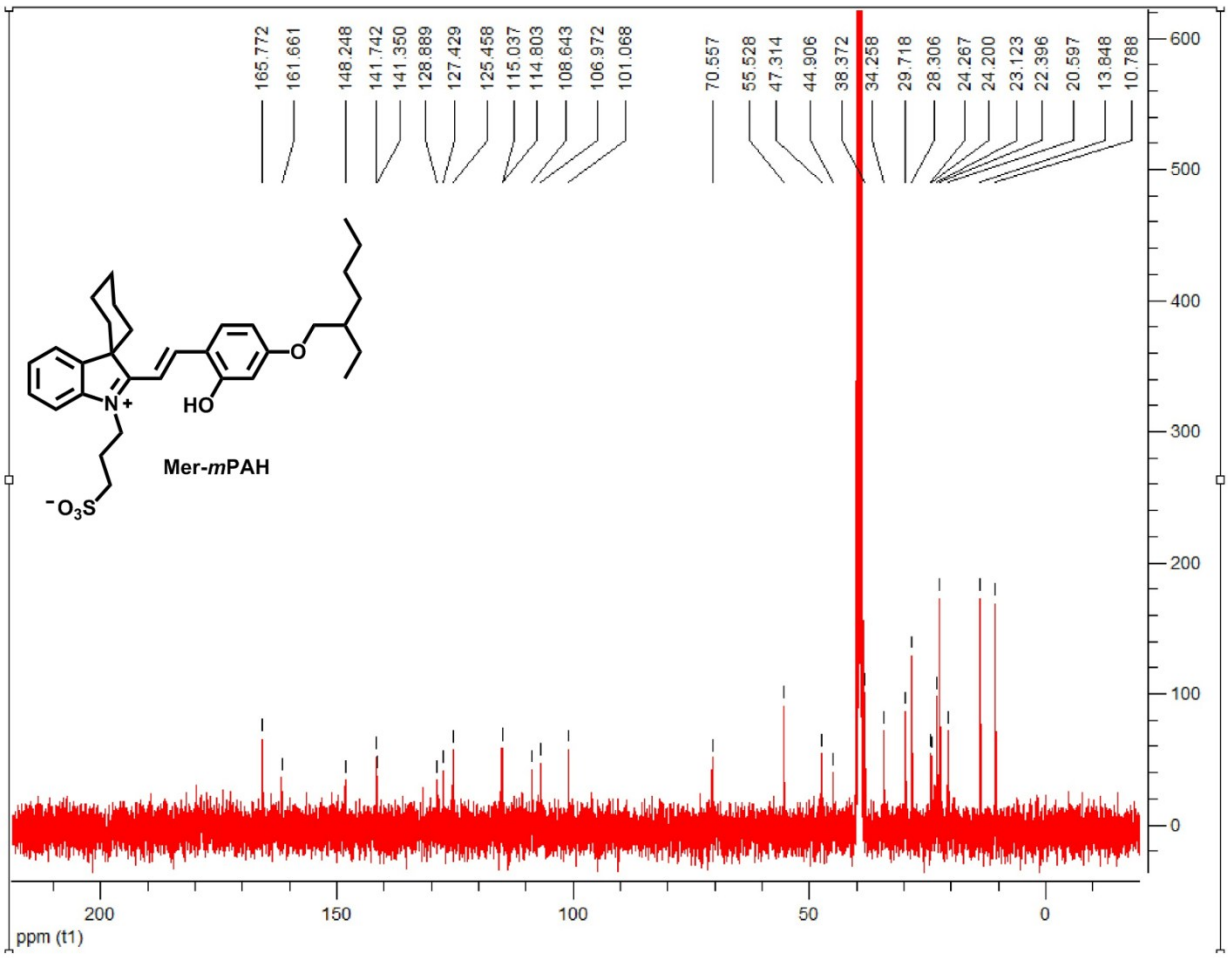

Fig. S6 ^{13}C NMR spectra of **Mer-*m*PAH**.

3. DFT/TD-DFT calculations

All calculations were performed using the Gaussian 09 package.[6] The visualizations were obtained using the Avogadro 1.2.0n software.[7] All calculations including the geometry optimizations, the frequency calculations, and the time-dependent single point energy calculations were carried out with the B3LYP global hybrid functional using the 6-311++G (2d,p) basis set.[8] Ethanol was accounted as an implicit solvent using the IEFPCM solvation model.[9]

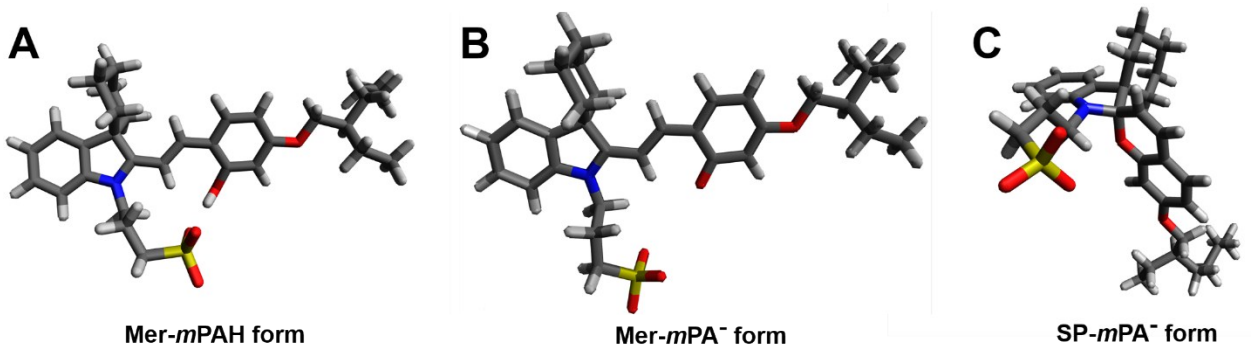

Fig. S7. Optimized geometries for ground state structure of (A) Mer-*m*PAH, (B) Mer-*m*PA$^-$, and (C) SP-*m*PA$^-$ forms.

Gibbs-free energy calculations

The Zero-Point Energy (ZPE) corresponds to the energy of a system where the molecular vibrations that persist at 0K are taken into consideration.[10] To obtain the Gibbs-free energies of *m*PAH in its different states, we performed frequency calculations on the optimized structures of Mer-*m*PAH, Mer-*m*PA$^-$, and SP-*m*PA$^-$. Then, the energy of the system in its different states was computed as follows:

(1) $\Delta G_{\text{Mer-}m\text{PAH}} = ZPE_{\text{Mer-}m\text{PAH}} = -5446010.5$ kJ/mol

(2) $\Delta G_{\text{Mer-}m\text{PA}^-} = ZPE_{\text{Mer-}m\text{PA}^-} + \Delta G_{\text{Solvated H}^+} = (-5444831.6 \text{ kJ/mol}) + (-1104.5 \text{ kJ/mol})$

$= -5445936.1$ kJ/mol

(3) $\Delta G_{\text{SP-}m\text{PA}^-} = ZPE_{\text{SP-}m\text{PA}^-} + \Delta G_{\text{Solvated H}^+} = (-5444818.3 \text{ kJ/mol}) + (-1104.5 \text{ kJ/mol})$

$= -5445922.761$ kJ/mol

All the ΔG were normalized to $\Delta G_{\text{Mer-}m\text{PAH}}$ as follows:

(4) Normalized $\Delta G_{\text{Mer-}m\text{PAH}} = \Delta G_{\text{Mer-}m\text{PAH}} - \Delta G_{\text{Mer-}m\text{PAH}} = 0$ kJ/mol

(5) Normalized $\Delta G_{\text{Mer-}m\text{PA}^-} = \Delta G_{\text{Mer-}m\text{PA}^-} - \Delta G_{\text{Mer-}m\text{PAH}} = 74.4$ kJ/mol

(6) Normalized $\Delta G_{\text{SP-}m\text{PA}^-} = \Delta G_{\text{SP-}m\text{PA}^-} - \Delta G_{\text{Mer-}m\text{PAH}} = 87.8$ kJ/mol

Note that the energy of a solvated proton must be added to the Mer-*m*PA$^-$ and SP-*m*PA$^-$ forms in order to make all the Gibbs free energies comparable. The value for the Gibbs free energy for a solvated proton in aqueous media was obtained from Tissander *et al* seminal work on solvated ions.[11] Unfortunately, there is no paper that follows Tissander *et al* procedure on calculating the Gibbs free energy of a solvated proton in ethanol via cluster calculations. Nonetheless, Markovic *et al* provide Gibbs free energy calculations for

a solvated proton in ethanol (and many other solvents) using accurate calculations.[12] Although their work does not feature a fully comprehensive solvation model for the proton, it does go on to show that the Gibbs free energies for solvated protons are not so far in water and in ethanol (-1055.8 kJ/mol and -1064.9 kJ/mol, respectively). Hence, we choose to approximate the solvation Gibbs free energy for a proton in ethanol, or in an ethanol-water mixture, by the highly accurate reported value by Tissander *et al*. It is important to recognize that the predicted energy for the Mer-*m*PA$^-$ might have a significant error, since the model does not seem to be able to fully account for its electronic structure (refer to Fig S.8B).

For completion, we repeated the same process for an aqueous solution. All structures were optimized with B3LYP/6-311++G(2d,p) accounting for water as a solvent using the IEFPCM model. A frequency calculation using those same parameters was performed to obtain the ZPE-corrected Gibbs-free energies. The energy of the system (in water) in its different states was computed as follows:

(1) $\Delta G_{\text{Mer-}m\text{PAH}} = ZPE_{\text{Mer-}m\text{PAH}} = -5446016.3$ kJ/mol

(2) $\Delta G_{\text{Mer-}m\text{PA}^-} = ZPE_{\text{Mer-}m\text{PA}^-} + \Delta G_{\text{Solvated H}^+} = (-5444833.3 \text{ kJ/mol}) + (-1104.5 \text{ kJ/mol})$

$= -5445937.8$ kJ/mol

(3) $\Delta G_{\text{SP-}m\text{PA}^-} = ZPE_{\text{SP-}m\text{PA}^-} + \Delta G_{\text{Solvated H}^+} = (-5444828.8 \text{ kJ/mol}) + (-1104.5 \text{ kJ/mol})$

$= -5445933.3$ kJ/mol

All the ΔG were normalized to $\Delta G_{\text{Mer-}m\text{PAH}}$ as follows:

(4) Normalized $\Delta G_{\text{Mer-}m\text{PAH}} = \Delta G_{\text{Mer-}m\text{PAH}} - \Delta G_{\text{Mer-}m\text{PAH}} = 0$ kJ/mol

(5) Normalized $\Delta G_{\text{Mer-}m\text{PA}^-} = \Delta G_{\text{Mer-}m\text{PA}^-} - \Delta G_{\text{Mer-}m\text{PAH}} = 78.5$ kJ/mol

(6) Normalized $\Delta G_{\text{SP-}m\text{PA}^-} = \Delta G_{\text{SP-}m\text{PA}^-} - \Delta G_{\text{Mer-}m\text{PAH}} = 83.0$ kJ/mol

Correlation between experimental and theoretical absorbance spectra

The first 40 excited states for Mer-*m*PAH, Mer-*m*PA$^-$, and SP-*m*PA$^-$ forms were calculated using time-dependent DFT on the previously optimized structures. The scales for the theoretical Mer-*m*PA$^-$ spectra seem disproportionate because there is a significant population of the *m*PAH in its SP-*m*PA$^-$ conformer (evidenced by the peak at 287 nm in the Mer-*m*PA$^-$ experimental spectra). If the experimental spectra contained solely Mer-*m*PA$^-$, the scales would be in better agreement. For example, refer to the spectra of the SP-*m*PA$^-$. The experimental spectrum shows no *m*PAH in its Mer-*m*PA$^-$ conformer (peak at 554 nm) and a negligible amount of *m*PAH in its Mer-*m*PAH conformer (peak at 474 nm). As a result, the scales of the theoretical and experimental spectra are much closer.

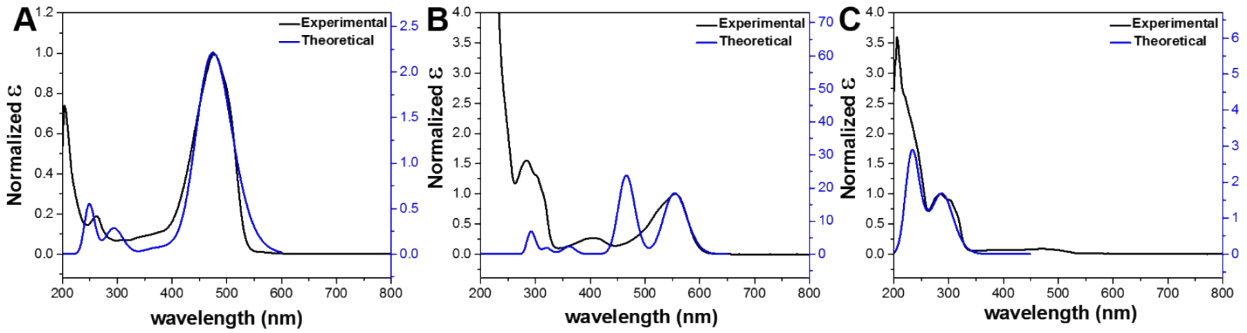

Fig. S8. Overlap of the normalized experimental absorption spectra (black line) and the shifter computed spectra (blue line; more details provided below) for (A) Mer-*m*PAH, (B) Mer-*m*PA$^-$, and (C) SP-*m*PA$^-$ forms.

The spectra in Fig. S8A were normalized to the peak corresponding to the Mer-*m*PAH form in the experimental spectrum in 100% ethanol. The theoretical spectra required a shift of -0.221 eV to match the experimental first electronic transition (from 437.91 nm to 474.91 nm). A FWMH of 0.21 eV was required to provide the best possible overlap.

The spectra in Fig. S8B were normalized to the peak corresponding to the Mer-*m*PA- form in the experimental spectrum in ethanol/water (50/50). The theoretical spectra required a shift of -0.282 eV to match the experimental first electronic transition (from 492.21 nm to 554.21 nm). A FWMH of 0.10 eV was required to provide the best possible overlap.

The spectra in Fig. S8C were normalized to the lowest energy electronic transition of the experimental spectrum in 100% ethanol. The theoretical spectra for SP-*m*PA$^-$ required a shift of 0.178 eV to match the experimental first electronic transition (from 300.24 nm to 287.23 nm). A FWMH of 0.33 eV was required to provide the best possible overlap.

The overlaps are good except in the case of Mer-*m*PA$^-$ form (Fig. S8B), where the transition corresponding to a shoulder in the experimental spectra is predicted to be at a considerable distance from the transition of lowest energy. As a result, the theoretical spectrum creates a new peak instead of a shoulder. This could be linked to the FWMH that is quite small in this case. A larger FWMH should merge these two peaks and lead to a better agreement. The inversion of the relative intensities of the two lowest transitions could also be an artifact due to a too crude model (B3LYP/6-311++G (2d, p)) or to the use of ethanol as the only solvent. Further investigations are required to give more insight on these issues.

4. Determination of thermodynamic acidity constant

The ground state acidity constant (pK$_a$) of metastable-state photoacid (*m*PAH) is determined by the following thermodynamic reaction provided below.

$$\boldsymbol{m}\mathbf{PAH} \underset{\text{Acid}}{\overset{\text{Base}}{\rightleftharpoons}} \boldsymbol{m}\mathbf{PA}^- + \mathbf{H}^+$$

Likewise, Henderson-Hasselbalch equation (Equation 1) was correlated with degree of protonation (Equation 2). Accordingly, mass-balance equation (Equation 3) was used to modify Equation 1 to Equation 4.

Equation 1: Henderson-Hasselbalch equation based of *m*PAH equilibrium reaction

$$pH = pK_a + \log\frac{[mPA^-]}{[mPAH]}$$

Equation 2: Degree of protonation, "α"

$$\alpha = \frac{[mPAH]}{[mPAH]_T} = \frac{A - A_D}{A_P - A_D}$$

Degree of protonation is defined as the ratio of acidic-open form *m*PAH, where subscript "T" signifies total concentration of *m*PAH. Likewise, the concentrations of acidic-open form *m*PAH can be related to absorbance as denoted by "A". The symbols "A_D" and "A_P" represents absorbance values of acidic-open form *m*PAH absorption peak when it is fully deprotonated and fully protonated.

Equation 3: Mass-balance equation

$$[mPAH]_T = [mPAH] + [mPA^-]$$

Note that, both conjugated basic forms (open and closed) of *m*PAH is denoted as "*m*PA$^-$".

Equation 4: Modified Henderson-Hasselbalch equation

$$pH = pK_a + \log\left[\frac{(1 - \alpha)}{\alpha}\right]$$

This theoretical equation was derived by rearranging Equation 1 by incorporation of both Equation 2 and Equation 3, and was used to fit the experimental for estimating the pK$_a$ of Mer-*m*PAH.

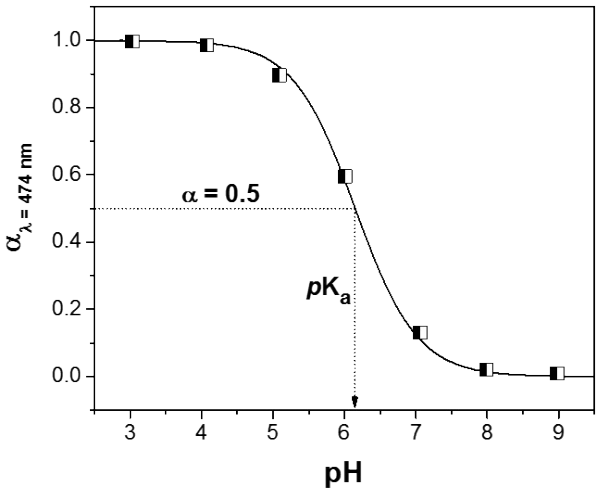

Fig. S11. Correlation between theoretical fitting and the obtained experimental data to estimate the thermodynamic acidity constant.

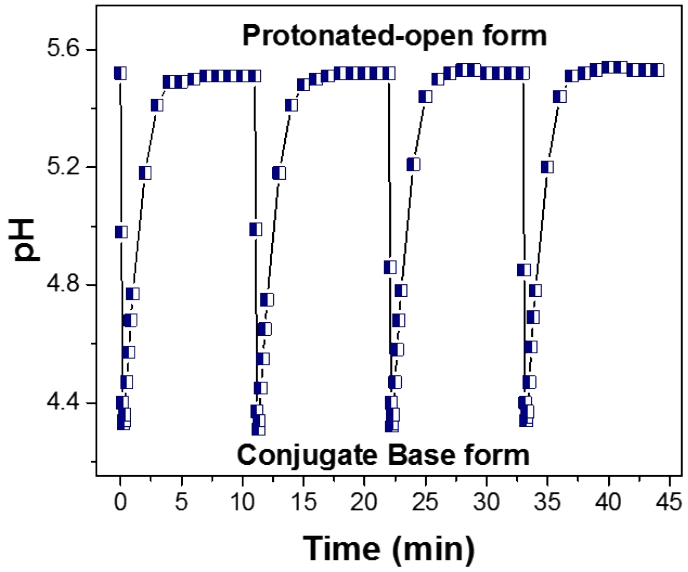

5. Additional Figures and Table

Fig. S12. Modulation of pH by 470 nm light over multiple cycles with respect to time for an ethanol/water (90/10) solution containing 65 µM of Mer-*m*PAH.

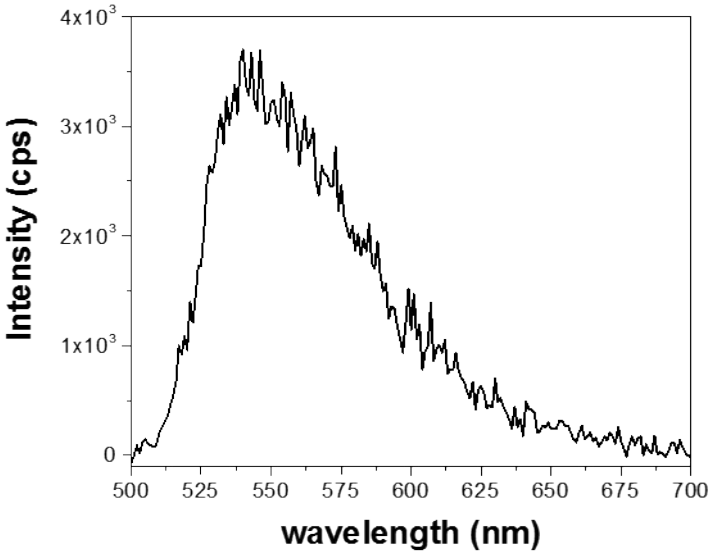

Fig. S13. Emission spectra for ethanol solution containing Mer-*m*PAH (6.50×10^{-5} M) only. Excitation wavelength 478 nm was used.

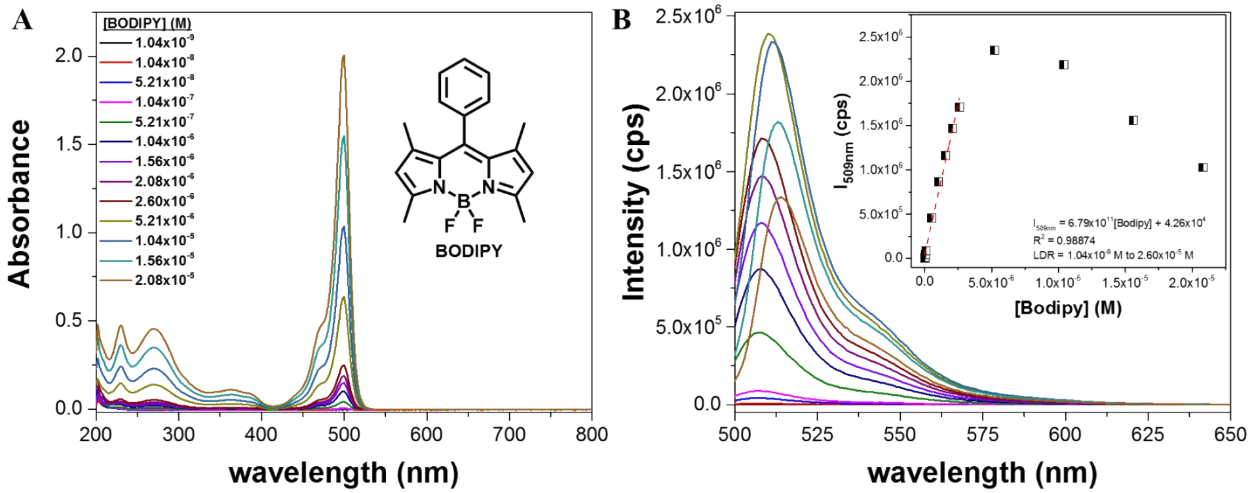

Fig. S14. Optical characteristics for different concentrations of BODIPY in ethanol. A) Absorbance spectra. B) Emission spectra (excitation wavelength was 495 nm) with calibration plot to illustrate self-quenching behaviour (Inset).

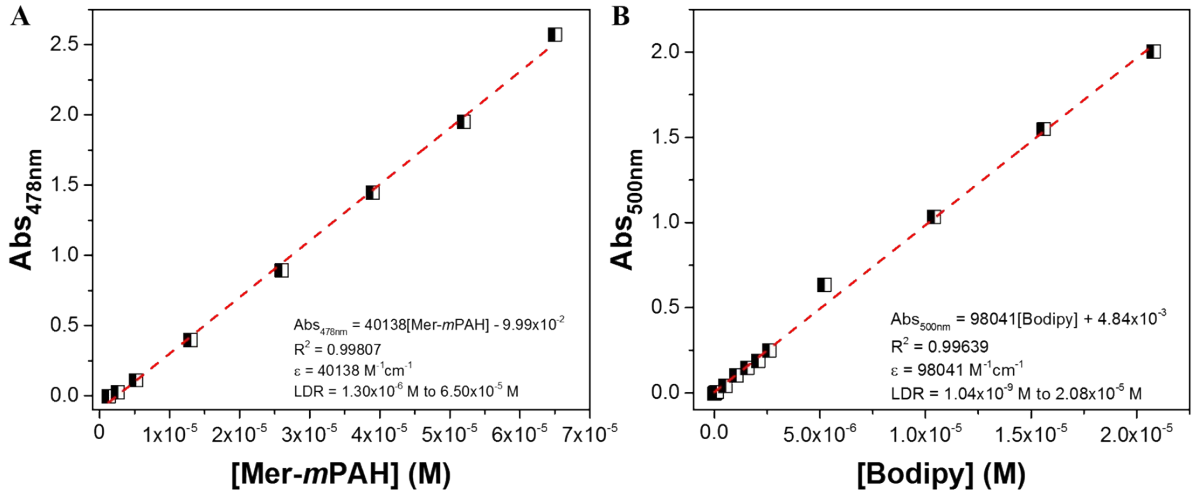

Fig. S15. Absorbance-based calibration plot for ethanol solutions containing different concentrations of A) Mer-*m*PAH (1.30x10^{-6} M, 2.60x10^{-6} M, 5.21x10^{-6} M, 1.30x10^{-5} M, 2.60x10^{-5} M, 3.90x10^{-5} M, 5.20x10^{-5} M and 6.50x10^{-5} M), and B) BODIPY (1.04x10^{-9} M, 1.04x10^{-8} M, 5.21x10^{-8} M, 1.04x10^{-7} M, 5.21x10^{-7} M, 1.04x10^{-6} M, 1.04x10^{-6} M, 1.56x10^{-6} M, 2.08x10^{-6} M, 2.60x10^{-6} M, 5.21x10^{-6} M, 1.04x10^{-5} M, 1.56x10^{-5} M and 2.08x10^{-5} M).

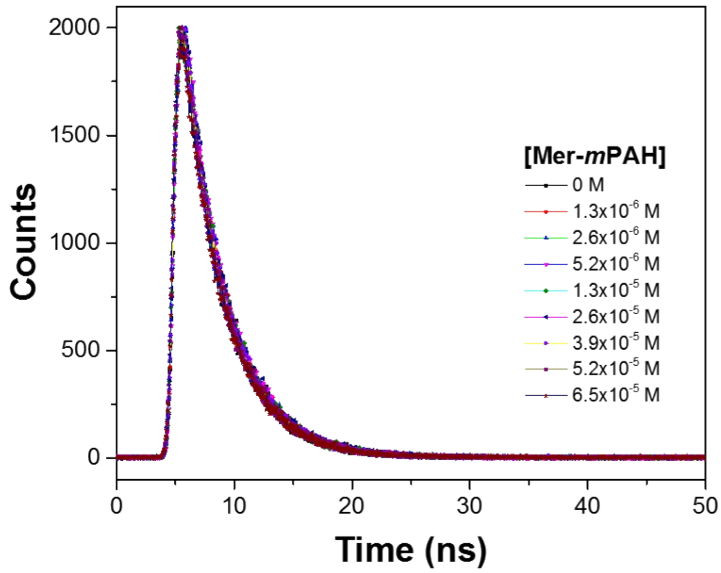

Fig. S16. Lifetime decay profiles for ethanol solutions containing fixed concentration of BODIPY (2.60×10^{-6} M) with different concentrations of Mer-*m*PAH.

Table S1. Lifetime decay data for different concentration of Mer-*m*PAH with fixed concentration of BODIPY.

[Mer-*m*PAH] + 2.6×10^{-6} M BODIPY	τ (ns)
0 M	3.317 [a]
1.3×10^{-6} M	3.328
2.6×10^{-6} M	3.321
5.2×10^{-6} M	3.320
1.3×10^{-5} M	3.326
2.6×10^{-5} M	3.294
3.9×10^{-5} M	3.316
5.2×10^{-5} M	3.295
6.5×10^{-5} M	3.315

[a] τ_0

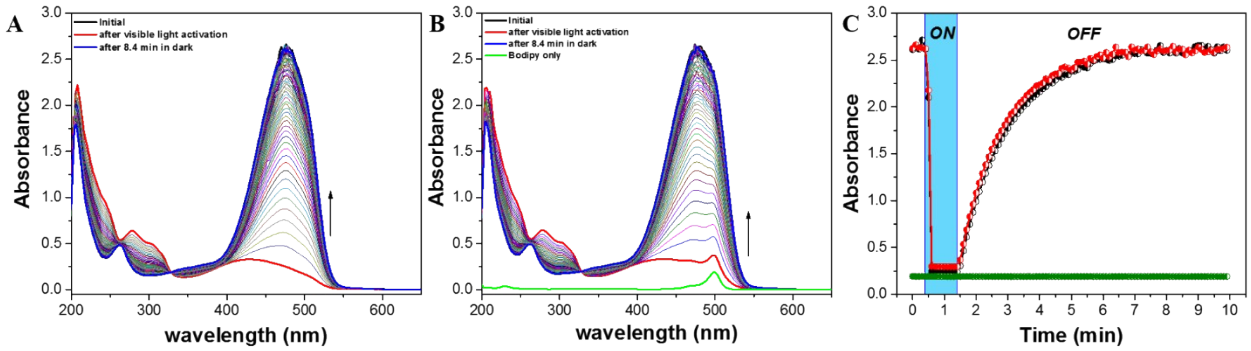

Fig. S17. Absorbance-based experiments for ethanol solution containing A) 6.50x10^{-5} M of Mer-*m*PAH, B) 6.50x10^{-5} M of Mer-*m*PAH with 2.60x10^{-6} M of BODIPY (in green: absorbance spectra of 2.60x10^{-6} M of BODIPY), and C) Kinetic plots for a solution of 6.50x10^{-5} M Mer-*m*PAH only (in black, λ_{abs} = 478 nm), 2.60x10^{-6} M BODIPY with 6.50x10^{-5} M Mer-*m*PAH (in red, λ_{abs} = 478 nm), and 2.60x10^{-6} M BODIPY only (in green, λ_{abs} = 500 nm) (*ON* region signifies visible light activation by 470 nm light, while the *OFF* region signifies in the dark).

6. References

[1] Y. Chen, J. Zhao, H. Guo, L. Xie, *J. Org. Chem*. **2012**, *77*, 2192.
[2] C. R. Bhattacharjee, G. Das, P. Mondal, *J. Coord. Chem.* **2011**, *64*, 3273.
[3] E. A. Owens, N. Bruschi, J. G. Tawney, M. Henary, *Dyes Pigm.* **2015**, *113*, 27.
[4] A. Alagumalai, M. K. Munavvar Fairoos, P. Vellimalai, M. C. Sil, J. Nithyanandhan, *ACS Appl. Mater. Interfaces* **2016**, *8*, 35353.
[5] Z. Shi, P. Peng, D. Strohecker, Y. Liao, *J. Am. Chem. Soc*. **2011**, *133*, 14699.
[6] M. J. Frisch, G. W. Trucks, H. B. Schlegel, G. E. Scuseria, M. A. Robb, J. R. Cheeseman, G. Scalmani, V. Barone, B. Mennucci, G. A. Petersson, H. Nakatsuji, M. Caricato, X. Li, H. P. Hratchian, A. F. Izmaylov, J. Bloino, G. Zheng, J. L. Sonnenberg, M. Hada, M. Ehara, K. Toyota, R. Fukuda, J. Hasegawa, M. Ishida, T. Nakajima, Y. Honda, O. Kitao, H. Nakai, T. Vreven, J. A. Montgomery Jr., J. E. Peralta, F. Ogliaro, M. Bearpark, J. J. Heyd, E. Brothers, K. N. Kudin, V. N. Staroverov, T. Keith, R. Kobayashi, J. Normand, K. Raghavachari, A. Rendell, J. C. Burant, S. S. Iyengar, J. Tomasi, M. Cossi, N. Rega, J. M. Millam, M. Klene, J. E. Knox, J. B. Cross, V. Bakken, C. Adamo, J. Jaramillo, R. Gomperts, R. E. Stratmann, O. Yazyev, A. J. Austin, R. Cammi, C. Pomelli, J. W. Ochterski, R. L. Martin, K. Morokuma, V. G. Zakrzewski, G. A. Voth, P. Salvador, J. J. Dannenberg, S. Dapprich, A. D. Daniels, O. Farkas, J. B. Foresman, J. V. Ortiz, J. Cioslowski, D. J. Fox, *Gaussian, Inc.*, Wallingford CT, **2013**.
[7] M. D. Hanwell, D. E. Curtis, D. C. Lonie, T. Vandermeersch, E. Zurek, G. R. Hutchison, *J. Cheminf*., **2012**, *4*, 17.
[8] A. D. Becke, *J. Chem. Phys.*, **1993**, *98*, 1372.
[9] M. Cossi, G. Scalmani, N. Rega, V. Barone, *J. Chem. Phys*., **2002**, *117*, 45.
[10] J. B. Foresman, A. E. Frisch, *Exploring Chemistry with Electronic Structure Methods*, Gaussian Inc., Pittsburgh PA, **1993**.
[11] M. D. Tissander, K. A. Cowen, W. Y. Feng, E. Gundlach, M. H. Cohen, A. D. Earhart, J. V. Coe, T. R. Tuttle, *J. Phys. Chem. A*, **1998**, *102*, 7787.
[12] Z. Markovic, J. Tošovic, D. Milenkovic, S. Markovic, *Comput. Theor. Chem.*, **2016**, *1077*, 11.